Tim Karberg & Jana Eger-Karberg

A View on the "Father of Iron" from Space

The potential of multi-spectral earth observation data analysis for the detection of iron smelting facilities in between Jebel Haraza and Jebel Abu Hadid, Northern Kordofan[1]

This paper is dedicated to the memory of Prof. Ibrahim Musa (1953 – 2024)

Preface

The idea for a comprehensive study on the distribution of iron smelting facilities in Northern Kordofan and their spatial relation to other settlement and agricultural installations, especially terraced farming, was developed together with Ibrahim Musa, then dean of the faculty of archaeology and tourism, when the authors spent the winter term 2018/19 at the Al Neelain University, Khartoum. After postponing a joint project on that topic due to the COVID-19 pandemic and the political developments in Sudan since then, the sad news of Ibrahim Musa's death in January this year ended these plans. Nevertheless, the authors benefitted to an inestimable extent from the fruitful scientific debates with Ibrahim Musa on that topic – therefore, many of his ideas also influenced the research this paper is based on.

1. Introduction

The research project "InterLINK - Interregional Linkage Investigations in Northern Kordofan" of the University of Muenster's Research Centre Ancient Sudan investigates possible connections between the ancient and medieval cultures of the Nile Valley and their nearer and more distant neighbours in the west. The aim is to investigate whether and to what extent states such as the Napatan and Meroitic empires or the medieval states of Makuria or Alwa reached out into their western periphery, and what kind of contacts with the early cultures of Kordofan, Darfur and the Chad Basin resulted from this. In the context of this research, the Cushite and Nubian cultures are to be understood not only as Nile Valley cultures oriented along an imaginary north-south axis, but also as "Sudanic" Sahel cultures that were integrated into an east-west axis of cultural and economic exchange processes.[2]

The semi-arid region of Northern Kordofan in Sudan shows a rich history of iron smelting, i.e. around the hills of Jebel Haraza and Jebel Abu Hadid.[3] Standard methods of archaeological survey are often constrained by geographical vastness, resource limitations, and accessibility issues, especially since the outbreak of the full-scale war in Sudan in April 2023. In response, this study employs multi-spectral satellite data analysis as a novel approach to detect and map the remnants of iron smelting activities.

The potential of satellite based earth observation methods combined with spatial statistics in archaeology has been demonstrated in various contexts;[4] however, its application in detecting ferrous metallurgy remains underexplored. The spectral properties of surface material altered by ancient smelting processes could provide vital clues observable through remote sensing technologies.

1.1. Study area

Jebel Haraza and Jebel Abu Hadid ('Father of Iron') are located in the southwestern part of the InterLINK concession area in the Sudanese state of Northern Kordofan. Jebel Haraza is located at

1 This paper is based on a presentation at this year's "Computer Applications and Quantitative Methods in Archaeology" German chapter workshop, held in Münster, September 5th 2024. The authors express their gratitude to the participants of this workshop for the lively discussion of the preliminary results of this research.

2 Eger-Karberg & Karberg, 2022

3 Spaulding, 1998

4 Cf. Eger & Karberg, 2020; Eger-Karberg & Karberg, 2021; Eger-Karberg & Karberg, 2024

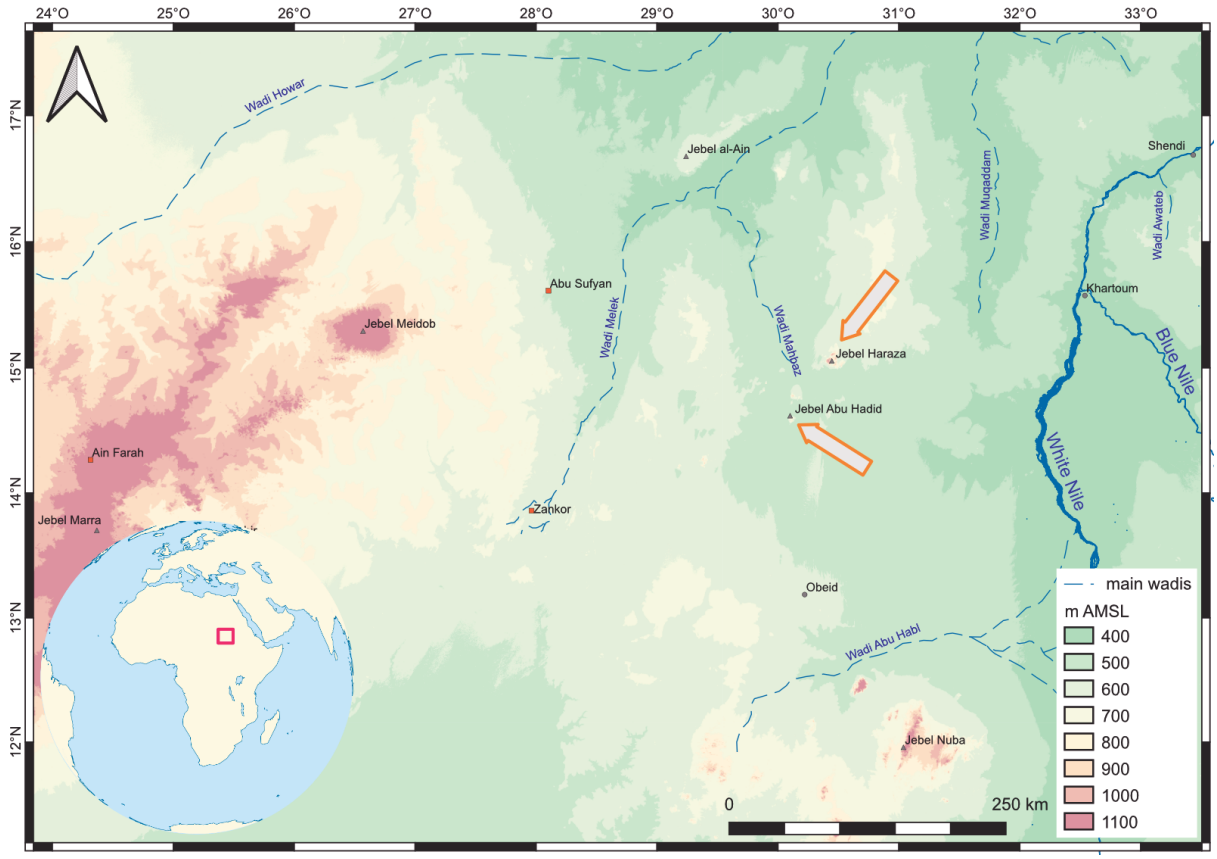

Fig. 1: Map of Northern Kordofan and adjacent areas. Arrows mark the Jebel Haraza and Jebel Abu Hadid study area. Topographical elevation data derived from ALOS DEM (© JAXA).

15°03'N 30°26'E, and Jebel Abu Hadid at 14°35'N 30°07'E (Fig. 1). For both areas, individual evidence of historical iron smelting was found (see below). These also coincide with historical sources. However, a comprehensive mapping of the iron slags and thus of the entire iron smelting areas at Jebel Haraza and Jebel Abu Hadid has not yet been possible on the ground - a desideratum that cannot be eliminated by archaeological research on the ground for the time being due to the current situation in Sudan and especially in Kordofan.

1.2. Previous research

Iron smelting on a local level in Northern Kordofan was already mentioned by travellers visiting the area during the 19th century and documenting traditional customs. Especially the local production of iron weeding tools as well as small models of these tools used as local currency is well documented.[5]

Remnants of ancient iron works were already observed by Harold A. MacMichael.[6] He describes remains of iron workshops with sherds of ceramic tuyères as well as "refuse […] thrown on top of the [workshop's] backwalls", which most presumably refers to slag. While he also presents a black/white landscape photo showing the area of the iron workshops,[7] he gives only very rough hints for the location of these findspots. He locates them at a place named "*Arangóg on the south of El Haráza*"[8], but a locality with this name is not marked on the map within his own book.[9] It also does not correspond to modern place names in the most detailed topographic maps available for the region.[10] The online gazetteer 'geonames' lists a hill named "*Arangol*".[11] The vicinity of this hill, however, no landscape elements resembling his published picture are present, therefore this localisation is merely to be seen as an

5 I.e. Holroyd, 1839
6 MacMichael, 1912 (reprint 2010), p. 95
7 MacMichael, 1912 (reprint 2010), Plate III
8 MacMichael, 1912 (reprint 2010), p. 95
9 MacMichael, 1912 (reprint 2010), attached map in book pocket
10 Cf. i.e. United Nations Office for the Coordination of Humanitarian Affairs, 2015, or General Staff of the Armed Forces of the USSR, 1979, sheet D-36-A, which are the most comprehensive topographic maps of this region.
11 https://www.geonames.org/7465572/arangol.html

approximate indication of the nearest known place name.

In 1993, a research group of the Technical University Berlin led by Rainer Fiedler-Volmer visited the area of the Jebel Haraza and the Jebel Abu Hadid.[12] The main aim of this field research were geo-tectonic investigations of the Es-Safya graben system.[13] As a side research project, they also probed a slag heap near a locality named "Tuba" in the Jebel Haraza region.[14] The place name "Tuba" can, as well as the locality "Arangóg", not be identified clearly on common topographic maps,[15] and can also not be identified via the 'geonames' gazetteer. Nevertheless, it is labelled as situated "*in einem weiten Talkessel im Inneren des Gebirges*",[16] so that at least some indications to narrow down the location are present. Even if there was no documentation done according to archaeological standards, individual slags were sampled.[17] Besides geochemical analysis, also some C^{14} dates were taken, dating the sampled slag heap from Jebel Abu Hadid with 68% probability between 1120 and 1260 AD, and with 95% probability between 1030 and 1280 AD.[18]

In 2018, a survey of the InterLINK project conducted by the authors focused on the western slopes of the Jebel Haraza and the Jebel Abu Hadid. Here, also some remains of iron slag were documented,[19] but the abovementioned iron smelting installations could not be found again due to the sparse information available.[20]

1.3. Research questions

In this paper, we investigate the potential of satellite-based earth observation methods to document ancient iron smelting sites. Since these sites are characterized by large amounts of iron slag, the idea evolved that the spectral signatures of specific diagnostic mineral components of iron slag could be analysed in order to identify them at the terrain surface. Our research aims to delineate these spectral signatures using multi-spectral imagery from satellites such as Sentinel-2, which is openly available for scientific purposes. This paper focuses on the development of spectral indices capable of detecting iron slag concentrations, and describes some ongoing research whether the spectral bands and resolution of this satellite data is sufficient to undertake this analysis. In this paper, some approaches to relocalize the iron smelting installations described by Harold A. MacMichael and Rainer Fiedler-Volmer (in the context of the sparse topographical information available from their publications) are presented and evaluated.

2. Datasets and methodology

2.1. Methodology

The approach for detecting iron slag concentrations within the soil surfaces is the adaption of the common method of normalized differential indication (NDI) to the specific mineralogical composition of iron slag from Sudan. In general, this type of spectral indices is used for landscape ecological questions (i.e. the Normalized Difference Vegetation Index to identify and classify surface cover by different vegetation),[21] but approaches for geological questions, for example the indication of iron ore deposits,[22] were also developed. In general, normalized differential indices follow the form

$$NDI_X = \frac{R_{max} - R_{min}}{R_{max} + R_{min}}$$

which means that the spectral (metrically scaled) raster attribute value of the wavelength which shows the minimum reflectance characteristics at the surface of the material in question (R_{min}) is in a first step subtracted from the attribute value with the maximum reflectance characteristics of the respective material (R_{max}), as a second step both are added to each other, and third the result of the first calculation step is divided by the second.[23]

While idices using this type of formula pattern are meanwhile widespread in landscape ecological and agricultural research, their application on minerals still developing. Since to the knowledge of the authors a specific formula for diagnostic mineral components of iron slag does not exist for the time being, the first step of our research was the

12 Fiedler-Volmer, 1998, pp. 26-25
13 Fiedler-Volmer, 1998, pp. 4-6
14 Fiedler-Volmer, 1998, p. 28
15 Cf. Fn. 10.
16 Fiedler-Volmer, 1998, p. 28
17 Fiedler-Volmer, 1998, pp. 32-36
18 Fiedler-Volmer, 1998, p. 36
19 Due to administrative obstacles it was not possible to probe and analyse samples from there in 2018.
20 Eger & Karberg, 2019, p. 137
21 Tucker, 1979
22 Mielke, et al., 2014, pp. 95-97
23 Formulas following this pattern are i.e. used by the Normalized Difference Vegetation Index NDVI (Tucker, 1979), the Soil Adjusted Vegetation Index SAVI (Huete, 1988), and the Normalized Difference Water Index NDWI (Gao, 1996).

development of a reliable attempt for such an index. Therefore, the specifications of the composition of Sudanese iron slags make a structural further methodological development necessary. The definition of such an index followed the spectral albedo (relative spectral reflectance) signatures of diagnostic mineral components according to their documentation in the most comprehensive openly available scientific database of mineralogical spectral profiles, which is provides by the United States Geological Survey Authority (USGS).[24] After defining a useful Normalized Difference Index, it is applied to multispectral data of the Sentinel-2 satellite's Multispectral Instrument (MSI) provided by the Copernicus Earth Observation Program.[25] Since the browser-based online database tool uses an access interface based on Java script, the analytical scripts in this paper are carried out in Java.

Concerning the chemical-mineralogical composition of Sudanese iron slags, samples from the Royal City of Meroe are most comprehensively studied. First archaeometallurgical investigations were carried out during the Meroe Joint Excavation already in 1993.[26] In recent times, comprehensive archaeometallurgical investigations at Meroe were carried out under the directorship of Jane Humphris.[27] While the results of both research projects differ in some detail, both point out that the iron slags from Meroe contain high amounts of fayalite (Fe_2SiO_4) and hercynite ($FeAl_2O_4$).[28] Other mineralogical components lack a clear differentiation potential from surrounding soils (i.e. FeO components which also occur in large quantities in the adjacent ferricrete sandstone).[29]

Another site with comprehensive archaeological investigations of iron smelting installations is Muweis. Here, also some slag samples were analysed chemically, resulting in similar concentrations of fayalite and hercynite.[30]

In order to index the concentration of these both diagnostic mineralogical components, their respective spectral profiles were evaluated from data provided by the USGS spectral library database. In this data sample collection, no specific samples of fayalite are listed, but several samples of the superordinate unit of mineralogical nomenclature, which is olivine (Mg_2SiO_4-Fe_2SiO_4). In order to get a spectral profile as close to the analysed slag samples as possible, the highly Fe_2-containing sample "Olivine HS285 Fo80"[31] was chosen. For hercynite, no spectral profile dataset was available in the USGS spectral library.

According to the chosen olivine sample, within the usable electromagnetic spectrum the maximum reflectance (R_{max}) with a relative value of 4.9 can be observed around λ = 550 nm, while the minimum reflectance (R_{min}) can be observed around λ = 1070 nm (Fig. 2). When applying the general pattern of normalized differential indices for multispectral analysis to this specific min/max albedo (relative spectral reflectance)[32] ratio, a first approach for a normalized difference fayalite/olivine index with a relative albedo difference (Δ_R) of 0.36 (on a 0-1 scale) could be:

$$NDI_{\mathrm{Fe2SiO4}} = \frac{R_{575\,nm} - R_{1070\,nm}}{R_{575\,nm} + R_{1070\,nm}} \triangleq \frac{0.49 - 0.13}{0.49 + 0.13} = 0.581$$

Unfortunately, such a formula would have a number of disadvantages. First, the spectral band B03 of the Sentinel-2 MSI covers λ = 575 nm quite well, since the centre λ of that band is set at 560 nm and its bandwidth measures 35 nm.[33] Anyway, no spectral band of that satellite system meets the λ = 1070 nm requirement. Band B09 is defined by a centre λ of 945 nm with a bandwidth of 20 nm, and band B10 by a centre λ of 1375 nm with a bandwidth of 30 nm,[34] both not covering λ = 1070 nm within the bandwidth. Therefore, the use of these bands for a normalized differential index reduces the relative albedo difference by 0.05 or 0.11 respectively (cf. Fig. 2). The second disadvantage is the low spatial resolution of bands B09 and B10 of (both) 60 m x 60 m per pixel,[35] while the spatial resolution of band B03 is 10 m x 10 m per pixel.[36] Since in any 10 m x 10 m pixel a specific value for the difference between the band albedo (relative reflectance) values can be calculated, the spatial resolution of the resulting index is 10 m x 10 m anyway, but the index values are levelled to some extent. Another characteristic of these spectral bands

24 Kokaly, et al., 2017
25 European Space Agency/Copernicus, 2024
26 Rehren, 1995
27 Carey, et al., 2019; Charlton & Humphris, 2019
28 Rehren, 1995, p. 23; Charlton & Humphris, 2019, pp. 904-905
29 Charlton & Humphris, 2019, p. 903
30 Dieudonné-Glad & Millet, 2021, pp. 6-7
31 Hunt, et al., 1973
32 "Spectral albedo" is a radiometric term defined as a non-dimensional value of the relative ratio between incoming radiation on a specific surface and the diffuse reflectance. Its values vary from 1, representing a (theoretical) perfect Lambertian scatterer, to 0, representing a (likewise theoretical) perfect Planckian body (Cf. Albertz, 2007, pp. 80-81).
33 ESA SUHET, 2013, p. 53
34 ESA SUHET, 2013, p. 54
35 ESA SUHET, 2013, p. 52
36 ESA SUHET, 2013, p. 51

with a major effect on the detection of mineralogical soil surface components is their sensitivity to water vapor. While band B09 has a high reflectance level for water vapor in the low atmosphere,[37] while band B10 is sensitive to water vapor in higher parts of the atmosphere, especially cirrus clouds (and therefore normally used as a correction band for this type of clouds).[38] A reliable workflow to detect iron slag from multispectral satellite data therefore has to ensure that the negative effects of water vapor on the results are minimized as much as possible.

While Sentinel-2 MSI band B09 is closer to the 1070 nm target value than band B10 and, additionally, the obfuscation by the effects of close-to-surface water vapor seems more manageable than cirrus clouds in higher atmospheric layers, tests were carried out with variants of the abovementioned normalized differential index for Fe_2SiO_4 anyway.

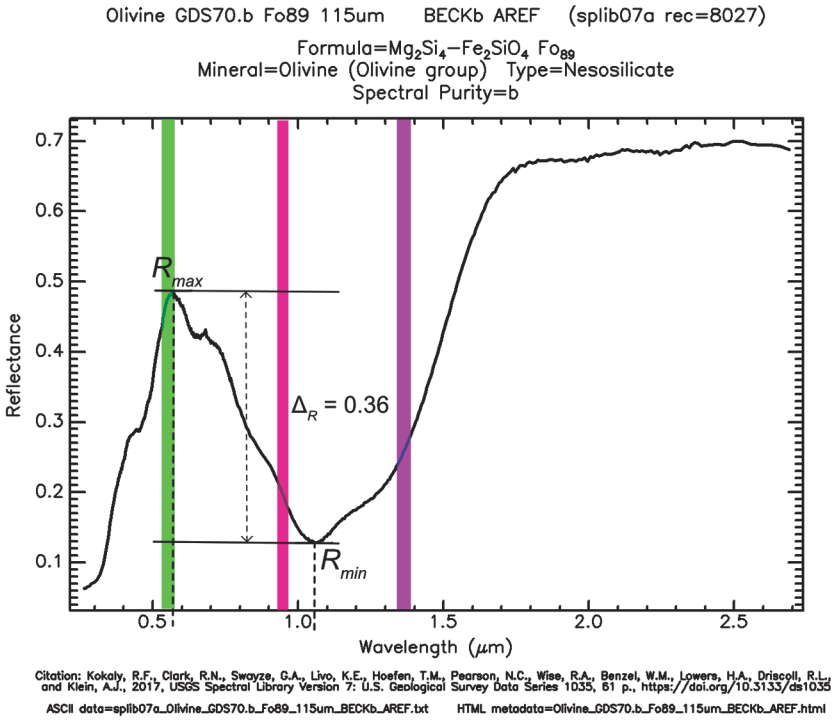

Fig. 2: Spectral profile of olivine sample HS285 Fo80 (provided by USGS Spectral Library Version 7 (Kokaly, et al., 2017)) with the spectral bandwidth of Sentinel-2 MSI band 3 (green), band 9 (rosé), and band 10 (purple). The maximum and minimum reflectance values (*Rmin* and *Rmax*) within the utilizable part of the electromagnetic spectrum are marked at reflectance values of 0.13 and 0.49.

The formulas used can be described as follows:

$$NDI_{\mathrm{Fe2SiO4\_}a} = \frac{B03 - B09}{B03 + B09}$$

and

$$NDI_{\mathrm{Fe2SiO4\_}b} = \frac{B03 - B10}{B03 + B10}$$

For the calculations in the interface of the Copernicus science hub database a java script code was used.[39] In the code, the respective values for the maximum calculated index value (*const maxIndex*) and the minimum calculated index value (*const minIndex*) were manually derived from the data attribution of the spectral bands in the Copernicus database.

The significance of the results was evaluated using a standard Moran's I index of spatial autocorrelation. This index is able to compute the clustering or dispersion of values, in this case the homogeneity of calculated index values of the suggested formula.[40] Therefore, we can estimate how unique and therefore significant the index values are concentrated compared to the surrounding area where high index values would be not connected to slag concentrations. In order to eliminate noise caused by external interference factors like water vapor, the spatial autocorrelation was calculated within a polygon area of interest (AOI) excluding cultivated land in order to narrow the results and keep their corruption by effects of low-atmospheric water vapor as small as possible. For that reason, the results of the index calculations for iron slag minerals were contextualised with index values of the normalized difference vegetation index.[41]

2.2. Earth observation datasets

Testing of the suggested index formula was done in two steps. First, the reliability of the method was estimated via a ground truth over a known concentration of iron slag, so that its functioning can be checked by external data. Second, after a successful ground truth,

37 Schläpfer, et al., 1998
38 ESA SUHET, 2013, p. 12
39 Cf. Appendix
40 Cf. Conolly & Lake, 2010, pp. 158-162. Spatial Autocorrelation is calculated using "System for Automated Geo-Scientific Analysis (SAGA) 9.3.2", tool "Global Moran's I for Grids 1.0" developed by Jan Papmeier, 2010.
41 Cf. Tucker, 1979

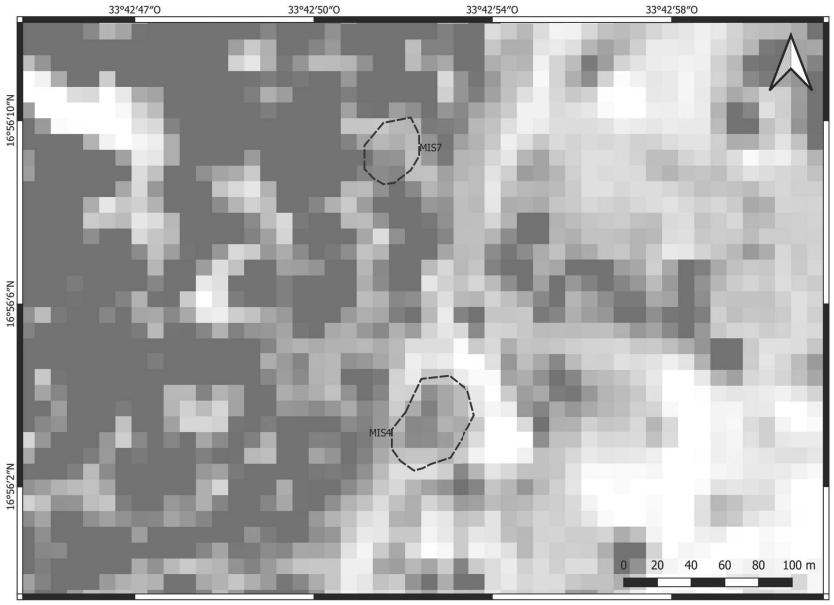

Fig. 3: Visualisation of NDIFe2SiO4_a values at the Royal City of Meroe, calculated from Sentinel-2 MSI dataset S2A_MSIL1C_20170329T080601_N0500_R078_T36QWD_20231110T103438. Location and designation of the iron slag accumulations after Carey, et al., 2019, p. 440 Fig. 5.

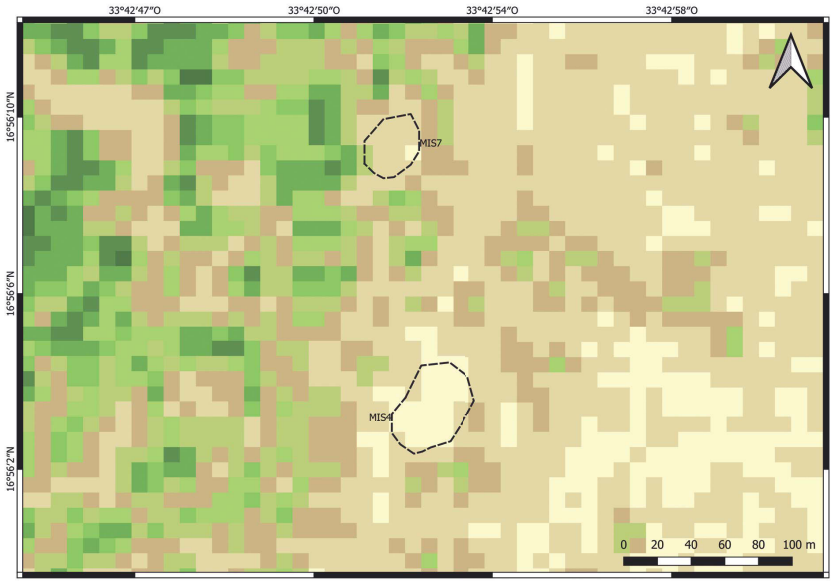

Fig. 4: Visualisation of NDVI values at the Royal City of Meroe, calculated from Sentinel-2 MSI dataset S2A_MSIL1C_20170329T080601_N0500_R078_T36QWD_20231110T103438. Location and designation of the iron slag accumulations after Carey, et al., 2019, p. 440 Fig. 5.

the actual experiment was carried out in unknown terrain. For the ground truth of the suggested indices, the area of the largest slag heaps of the Royal City of Meroe was chosen (named MIS4, MIS6, and MIS7 in the publications of the recent archaeometallurgical investigations in this area).[42] The size of these heaps made a clear spatial indication more likely regarding the relatively coarse spatial resolution of the Sentinel-2 MSI satellite data. In order to minimize the noise effect of water vapor, satellite data from dry weather conditions were chosen. For both multispectral data analyses (experiment at Jebel Haraza and ground truth at Meroe), datasets from the 2017 dry season were used. For the experiment, the dataset dates from February 20th 2017,[43] for ground truth it dates from March 29th, 2017.[44]

3. Results

The calculation of a normalized differentiation between band B03 and band B10 returned no statistically significant results during ground truth. At the other hand, the results of a normalized differentiation calculation between band B03 and band B09, which was at the beginning of the research believed to be more heavily affected by water vapor caused noise, returned more reliable results when tested for the ground truth area at the iron slag heaps of Meroe. The application of the proposed algorithm, at the very first glance, also did not provide a very clear differentiation between the observed slag heaps and other pixels (Fig. 3). But when contextualized with an index for vegetation density (Fig. 4), it became clear that most of the high index values outside the known slag concentrations on the ground were noise of water vapor caused by vegetational vaporisation, as already estimated in paragraph 2.1. When comparing the slag heap surface only with barren surrounding ground (i.e. with comparably low NDVI index values), a sig-

42 Carey, et al., 2019, p. 440 Fig. 5

43 S2A_MSIL1C_20170220T082001_N0204_R121_T36PTB_20170220T083406

44 S2A_MSIL1C_20170329T080601_N0500_R078_T36QWD_20231110T103438

nificant index value difference of ca. 0.05 was observed. When defining an area of interest only from pixels with comparably low NDVI values, a Moran's I spatial autocorrelation index of 0.690168 ('0' standing for a random spatial distribution, '1' for a perfect positive spatial clustering) proves the significance of the result.

After the general reliability of the methodological approach was shown by ground truth, the calculation was done for the Jebel Haraza dataset. Here, the results were even more clear. The proposed normalized difference index *a* for Fe_2SiO_4 showed highly significant differences from the surrounding areas, especially after subtracting high index values of NDVI. An example from the central Jebel Haraza shows the difference between a band combination representing the natural soil colour (Fig. 5), the NDVI index values (Fig. 6) and the calculated values of the proposed $NDI_{Fe2SiO4}$_a index (Fig. 7). Some of the highlighted spots correspond to areas of dense vegetation and can therefore be interpreted as water vapor noise, but at least two of the spots can be clearly delimited from vegetation and therefore are likely to represent iron slag. Since the two mentioned spots are located within a round valley which is situated between 70 m and 150 m lower than the surrounding rocky areas (and therefore fulfil the definition of a "*Talkessel*"), it may be identical with the slag heaps described by Rainer Fiedler-Vollmer.[45] The significance of the index value distribution patterns is shown by a Moran's I spatial autocorrelation index value of 0.941586 after defining an area of interest without vegetation cover.

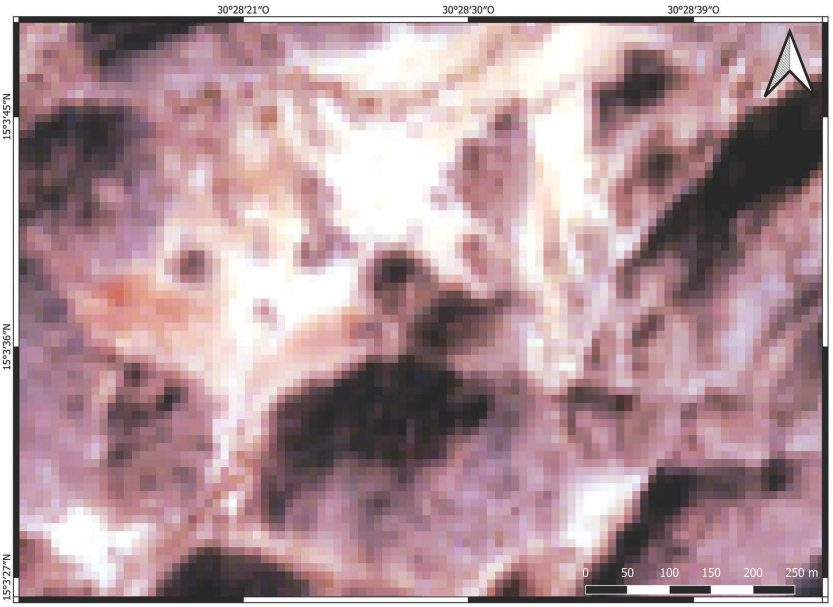

Fig. 5: Band combination resembling natural soil colour at Jebel Haraza. Clip from Sentinel-2 MSI dataset S2A_MSIL1C_20170220T082001_N0204_R121_T36PTB_20170220T083406.

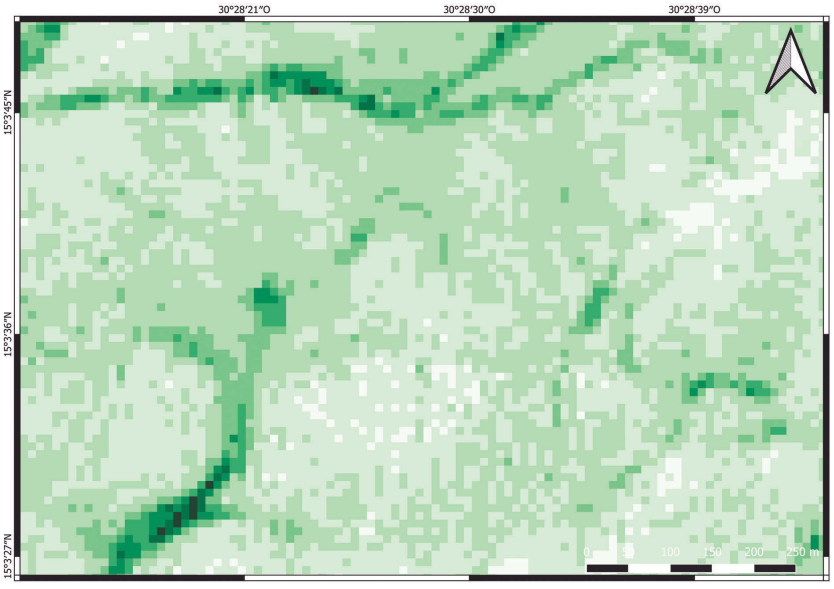

Fig. 6: Visualisation of NDVI values at Jebel Haraza, calculated from Sentinel-2 MSI dataset S2A_MSIL1C_20170220T082001_N0204_R121 T36PTB_20170220T083406.

4. Discussion

The ground truth as well as the experimental application of the proposed methodological approach proved the general possibility to identify iron slag by the systematic analysis of multispectral satellite data. Anyway, it also showed some specific disadvantages. First of all, the presence of water vapor in the low atmosphere is a major interference factor due to the spectral profile signatures of the most diagnostic mineral components of iron slag. Second, it was not possible to make use of the (theoretical) maximum

45 Fiedler-Volmer, 1998, p. 28

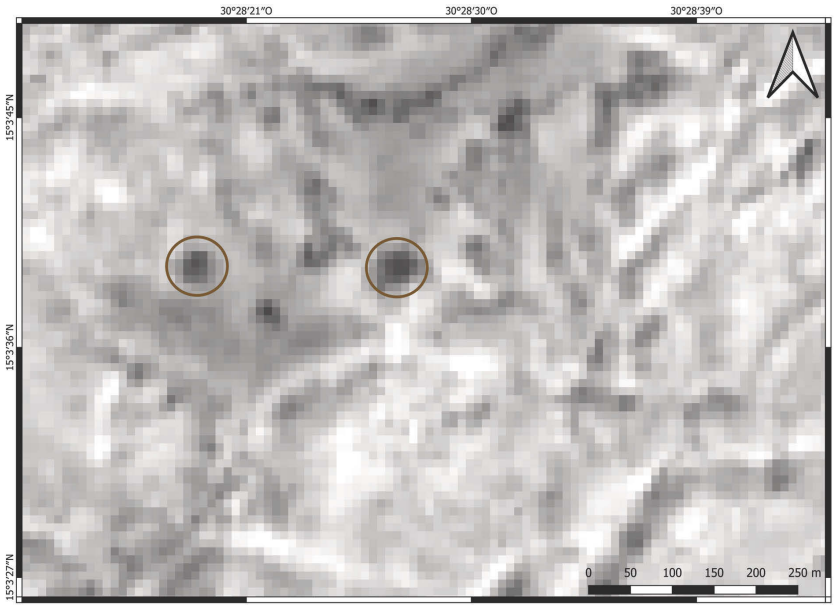

Fig. 7: Visualisation of NDIFe2SiO4_a values at Jebel Haraza, calculated from Sentinel-2 MSI dataset S2A_MSIL1C_20170220T082001_N0204_R121_T36PTB_20170220T083406. Highlighted spots of significant values of the suggested normalized difference index for iron slag components are marked with circles.

difference between the maximal and minimal spectral albedo values present in the spectral profile due to the band definitions of the Sentinel-2 Multispectral Instrument. This was caused by the centre wavelength and spectral bandwidth definition that was technically implemented in the MSI used by the Sentinel-2 satellites, and therefore indirectly connected to the first mentioned noise by water vapor, since the band definition of the MSI was technically designed in order to provide data which keep noise caused by atmospheric water vapor interferences as low as possible. Third, the coarse spatial resolution of band B09 of this satellite system further levelled the index result when calculating the difference between band B03 and band B09 values.

5. Conclusions and outlook

The application of the proposed method showed some remarkable results. Anyway, also some obstacles were observed, mainly because of external noise and the spatial resolution of the multispectral satellite imagery material available for this study. At least some of these disadvantages could be minimized by the provision of other satellite data with higher spectral and/or spatial resolution. For example, the Environmental Mapping and Analysis Program (EnMAP) of the German Aerospace Centre (DLR) provides a much higher spectral resolution (242 bands, which are arranged continuously without gaps like between bands B09 and B10 of the Sentinel-2 MSI).[46] Unlike the data from the Copernicus program, data from the EnMAP mission is not openly available to the scientific community, but has to be obtained from the DLR via an application procedure. We hope that in the near future we will be able to make use of this data for further research on the topic. But the continuous arrangement of the spectral bands can also cause more methodological challenges. Noise from sources like atmospheric water vapor (which is the practical reason for the gaps between the Sentinel-2 MSI spectral bands) might obfuscate the results, making even more careful meteorological preparation of the dataset selection necessary. Combined with improved satellite data this could lead to a systematic, semi-automated assessment of larger areas for the presence of historical iron slag.

Appendix

Java code for the application of

$$NDI_{\mathrm{Fe2SiO4\_}a} = \frac{B03 - B09}{B03 + B09}$$

```
function setup() {
  return {
    input: [„B03“,“B09“, „dataMask“],
    output: [
      { id:“default“, bands: 4 },
      { id: „index“, bands: 1, sampleType: ‚FLOAT32‘ }
    ]
  };
}
function evaluatePixel(samples) {
   let NDIFe2SiO4_a = (samples.B03-samples.B09)/
(samples.B03+samples.B09);
  const minIndex = -0.05;
  const maxIndex = 0.17;
  let visVal = null;
```

46 Deutsches Zentrum für Luft- und Raumfahrt, 2022

```
  if(NDIFe2SiO4_a  > maxIndex || index < minIndex) {
    visVal = [0, 0, 0, 0];
  }
  else {
    visVal = [...viz.process(index),samples.dataMask];
  }
```

Java code for the application of

$$NDI_{\mathrm{Fe2SiO4\_}a} = \frac{B03 - B09}{B03 + B09}$$

```
function setup() {
  return {
    input: [„B03“,“B10“, „dataMask“],
    output: [
      { id:“default“, bands: 4 },
      { id: „index“, bands: 1, sampleType: ‚FLOAT32‘ }
    ]
  };
}
function evaluatePixel(samples) {
  let NDIFe2SiO4_b = (samples.B03-samples.B10)/(samples.B03+samples.B10);
  const minIndex = 0.96;
  const maxIndex = 0.98;
  let visVal = null;
  if(NDIFe2SiO4_b  > maxIndex || index < minIndex) {
    visVal = [0, 0, 0, 0];
  }
  else {
    visVal = [...viz.process(index),samples.dataMask];
  }
```

Acknowledgements

The authors express their gratitude to Angelika Lohwasser and Huweida Ahmed for their support, and to Alexa Höhn, Fawzi Bakhiet, and Martin Oczipka for general discussions on and around the subject. The research is part of the "Interregional Linkage Investigations in Northern Kordofan" project, embedded in the DFG priority program "Entangled Africa". The authors express their gratitude to the coordination team and all other colleagues of this priority program for their manyfold support.

References

Albertz, J., 2007. *Einführung in die Fernerkundung - Grundlagen der Interpretation von Luft- und Satellitenbildern.* 3. ed. Darmstadt: Wissenschaftliche Buchgesellschaft.

Carey, C., Stremke, F. & Humphris, J., 2019. The ironworking remains in the royal city of Meroe: new insights on the Nile Corridor and the Kingdom of Kush. *Antiquity,* 93(368), pp. 432-449.

Charlton, M. & Humphris, J., 2019. Exploring ironmaking practices at Meroe, Sudan - a comparative analysis of archaeological and experimental data. *Archaeological and Anthropological Sciences,* Volume 11, pp. 895-912.

Conolly, J. & Lake, M., 2010. *Geographical Information Systems in Archaeology.* 4 ed. Cambridge: Cambridge University Press.

Deutsches Zentrum für Luft- und Raumfahrt, 2022. EnMAP - The German Spaceborne Imaging Spectrometer Mission. [Online] Available at: https://www.enmap.org/ [Accessed 12 04 2022].

Dieudonné-Glad, N. & Millet, M., 2021. Muweis, Sudan: Archaeometry of iron production at the end of Meroe Empire (2nd–4th centuries AD). *Journal of Archaeological Science: Reports,* Volume 38, p. 102892.

Eger, J. & Karberg, T., 2019. Neue Forschungen in Nord-Kordofan. Vorbericht über die Feldkampagnen des InterLINK-Projektes der Jahre 2017 und 2018. *Der antike Sudan. MittSAG*, Volume 30, pp. 131-146.

Eger, J. & Karberg, T., 2020. Nord-Kordofan im Satellitenbild. Vorbericht über die Forschungen des InterLINK-Projektes 2020. *Der antike Sudan. MittSAG*, Volume 31, pp. 87-98.

Eger-Karberg, J. & Karberg, T., 2021. Wasser für Gala Abu Ahmed. Ein Paläo-Drainagesystem zwischen Jebel Nagaschusch und Wadi Howar (Sudan) im Radar-Satellitenbild. *Der antike Sudan. MittSAG*, Volume 32, pp. 99-108.

Eger-Karberg, J. & Karberg, T., 2022. Interregional Linkage Investigations in Northern Kordofan (InterLINK). Report on the first project phase (2017-2022). *Sudan & Nubia*, Volume 26, pp. 82-93.

Eger-Karberg, J. & Karberg, T., 2024. The management of resources in remote desert areas: Bayuda and North Kordofan. In: R. Lemos & J. Budka, eds. *Landscape and resource management in Bronze Age Nubia: Archaeological perspectives on the exploitation of natural resources and the circulation of commodities in the Middle Nile.* Wiesbaden: Harrassowitz, pp. 34-45.

ESA SUHET, 2013. *Sentinel-2 User Handbook.* s.l.:ESA.

European Space Agency/Copernicus, 2024. Copernicus Science Hub. [Online] Available at: https://browser.dataspace.copernicus.eu/ [Accessed 28 08 2024].

Fiedler-Volmer, R., 1998. *Der Es Safya-Graben im Nordsudan - Geologie und Tektonik.* Berlin: FB Bauingenieurwesen und Angewandte Geowissenschaften der TU Berlin (Dissertation).

Gao, B.-C., 1996. NDWI - A normalized difference water index for remote sensing of vegetation liquid water from space. *Remote Sensing of Environment*, 58(3), p. 257–266.

General Staff of the Armed Forces of the USSR, 1979. *Ordnance Survey Map 1:200000, Sheet D-36-A.* Moskow: Главное управление геодезии и картографии при Совете министров СССР.

Holroyd, A. T., 1839. Iron Money of Kordofan. *The Numismatic Chronicle*, Volume 1, pp. 210-213.

Huete, A. R., 1988. A soil-adjusted vegetation index (SAVI). *Remote Sensing of Environment,* 25(3), pp. 295-309.

Hunt, G. R., Salisbury, J. W. & Lehnhoff, C. J., 1973. Visible and near-infrared spectra of minerals and rocks: VI. Additional silicates. *Modern Geology,* Volume 4, pp. 85-106.

Kokaly, R. et al., 2017. USGS Spectral Library Version 7: U.S. Geological Survey Data Series 1035. [Online] Available at: https://doi.org/10.3133/ds1035 [Accessed 30 04 2022].

MacMichael, H. A., 1912 (reprint 2010). *The Tribes of Northern and Central Kordofan.* Cambridge: Cambridge University Press.

Mielke, C. et al., 2014. Potential Applications of the Sentinel-2 Multispectral Sensor and the EnMAP Hyperspectral Sensor in Mineral Exploration. *European Association of Remote Sensing Laboratories E-Proceedings (EARSEeL eProceedings),* Volume 13, pp. 93-102.

Rehren, T., 1995. Meroe, Eisen und Afrika. *Mitteilungen der Sudanarchäologischen Gesellschaft zu Berlin e.V. (MittSAG),* Volume 3, pp. 20-25.

Schläpfer, D., Borel , C. C., Keller, J. & Itten, K. I., 1998. Atmospheric Precorrected Differential Absorption Technique to Retrieve Columnar Water Vapor. *Remote Sensing of Environment,* 65(3), pp. 353-366.

Spaulding, J., 1998. Early Kordofan. In: E. Stiansen & M. Kevane, eds. *Kordofan Invaded. Peripheral Incorporation and Social Transformation in Islamic Africa.* Leiden: Brill, pp. 46-59.

Tucker, C. J., 1979. Red and Photographic Infrared Linear Combinations for Monitoring Vegetation. *Remote Sensing of Environment*, 8(2), pp. 127-150.

United Nations Office for the Coordination of Humanitarian Affairs, 2015. *Sudan: North Kordofan State Administrative Map.* Genf/New York: OCHA.

Zusammenfassung

Während der Forschungen des InterLINK-Projektes in Nord-Kordofan wird intensiv daran gearbeitet, mit Hilfe von Fernerkundungsmethoden archäologische Befunde zu lokalisieren – aus Gründen effizienter Feldforschungsvorbereitung, derzeit aber leider vor allem aufgrund der vollständigen Unzugänglichkeit des zu erforschenden Gebietes. Als ein Ergebnis dieser Arbeiten wird hier ein Ansatz vorgestellt, historische Eisenverhüttungsinstallationen aufzuspüren. Zu diesem Zweck wurde ein Normalisierter Differenz-Index für diagnostische mineralische Komponenten typischer Eisenschlacken entwickelt und getestet. Hierbei zeigten sich erste erfolgversprechende Ergebnisse, aber auch Hindernisse, die bei der Weiterentwicklung dieser Methodik weiterer Forschung bedürfen.